J Nanopart Res (2023) 25:146
https://doi.org/10.1007/s11051-023-05771-w

RESEARCH PAPER

Exploration of the improving effect of Cd-doping on structural, photocatalytic, and biological properties of ZnO nanoparticles

B. Yalcin · L. Arda · I. E. Yalcin · K. Senturk · M. C. Alphan · D. Akcan · I. I. Ozyigit

Received: 31 December 2022 / Accepted: 18 May 2023 / Published online: 8 July 2023

Abstract ZnO and cadmium (Cd)-doped ZnO ($Zn_{1-x}Cd_xO$) nanoparticles with various compositions ($0.0 \leq x \leq 0.8$) were synthesized by sol-gel method. Structural, morphological, and photocatalytic properties as well as blood compatibilities of $Zn_{1-x}Cd_xO$ nanoparticles were investigated. While X-ray diffraction (XRD) applying the Rietveld refinement method was used to characterize the structural properties, scanning electron microscope (SEM) and transmission electron microscope (TEM) were used to investigate the surface morphology. It was found that the nanoparticles up to $x < 0.03$ Cd concentration had single phase of ZnO hexagonal wurtzite structure. Above $x \geq 0.03$ Cd concentration, two phases (ZnO and cadmium oxide (CdO)) were observed. SEM images with different magnifications revealed the dense, quasi-spherical, and agglomerated morphology of $Zn_{1-x}Cd_xO$ nanoparticles. The elemental compositions of $Zn_{1-x}Cd_xO$ nanoparticles have also been studied by EDX analysis. The photocatalytic activities and blood compatibilities of $Zn_{1-x}Cd_xO$ nanoparticles were studied by the photocatalytic degradation tests of crystal violet (CV) and hemolysis tests and respectively. In the photocatalytic activity tests, two samples $Zn_{0.90}Cd_{0.10}O$ and $Zn_{0.80}Cd_{0.80}O$ stood out with photodegradation percentages of 69.9% and 72.8%. Among the Cd-doped nanoparticles, the $Zn_{0.40}Cd_{0.60}O$ sample showed the highest blood compatibility with the weakest photocatalytic performance (degradation percentage; 32.2%). Structural properties, photocatalytic performance, and hemolytic potential of $Zn_{1-x}Cd_xO$ nanoparticles were investigated and compared with those of pure ZnO nanoparticles.

B. Yalcin
Department of Medical Laboratory Techniques, Vocational School of Health Services, Bahcesehir University, 34353 Istanbul, Türkiye

L. Arda (✉)
Department of Mechatronics Engineering, Faculty of Engineering and Natural Sciences, Bahcesehir University, 34353 Istanbul, Türkiye
e-mail: lutfi.arda@eng.bau.edu.tr

I. E. Yalcin
Department of Civil Engineering, Faculty of Engineering and Natural Sciences, Bahcesehir University, 34353 Istanbul, Türkiye

K. Senturk
Department of Mechatronics Engineering, Faculty of Engineering and Architecture, Istanbul Gelisim University, 34310 Istanbul, Türkiye

M. C. Alphan
Department of Electric Electronic Engineering, Faculty of Engineering and Natural Sciences, Bahcesehir University, 34353 Istanbul, Türkiye

D. Akcan
Department of Mathematics, Faculty of Engineering and Natural Sciences, Bahcesehir University, 34353 Istanbul, Türkiye

I. I. Ozyigit
Department of Biology, Faculty of Science, Marmara University, 34722 Istanbul, Türkiye

Keywords Sol–gel · Microstructure · Hemolysis · Photocatalytic activity · Nanoparticle · Biomedical relevance

Introduction

The design and fabrication of nano-size materials having unusual physical and chemical properties have gained much importance in the last decade. Especially, nano-sized metal oxides and their derivatives have been immensely studied due to their large surface area, good electrical and mechanical performances, and other superior properties arising from their dimensions [1–5].

As a valuable member of the nano-sized metal oxides family, ZnO possesses excellent UV absorbing properties, high quantum efficiency, unusual electrical, magnetic, and chemical properties [6–11]. In addition to the inherent physical properties of this wide band gap (3.3 eV) semiconductor, ZnO nanoparticles are also found to show antibacterial and anticancer activities due to their ability to induce the generation of reactive oxygen species (ROS) [12–15]. Moreover, ZnO nanoparticles have been approved as safe by the US Food and Drug Administration (FDA) and it has been emphasized that they can be used as effective drug delivery systems in various studies presented in the literature [16–19]. On the other hand, CdO, which has a band gap value of 2.5 eV, is an n-type semiconductor [20]. CdO nanoparticles have potential applications in optoelectronic devices, light-emitting diodes, gas sensors, and solar cells [21–23]. Photocatalytic and antibacterial properties were also observed for CdO nanoparticles synthesized by different methods [24, 25]. Both ZnO and CdO nanoparticles are used in biomedical applications such as bio-imaging, chemical sensors, and cancer treatment [26–30]. Thus, the main question here may be "how the biocompatibility of these individual materials changes when they take part in the same metal oxide matrix?". Anandhan et al. investigated the cytotoxicity of CdO nanoparticles and found a safe concentration range that is 1–5 μg mL^{-1} [31]. Another study conducted by Prashanth et al. focused on the hemocompatibility and anticancer activity of ZnO nanoparticles synthesized by the solution combustion method [32]. They found 1.56% and 5.44% hemolysis at 1.0 mg mL^{-1} and 5.0 mg mL^{-1} ZnO concentrations respectively. Additionally, they observed a reduction in the viability of breast cancer cells (MCF-7) at around 58% with 100 mg mL^{-1} ZnO treatment. Inhibitory effect of ZnO on renal carcinoma cells and its suppressive effect on cell proliferation and viability as well as the lipid accumulation was also reported [33].

Cd is a well-known element with proven toxic effects while the concentration of zinc directly affects the content of cadmium in the living systems [34]. These two elements show antagonistic interactions. Antagonism is the interaction between two or more compounds which the harmful effect is less than the predicted amount compared to the chemical applied alone. Various studies on plants and animals emphasize that the antagonism between Cd and Zn is due to their equivalent chemical affinity to the same biological systems [35–37]. In related literature studies, Cd, which is known to play a role in the carcinogenesis of different tissues such as pancreas, prostate, and liver, was evaluated in terms of its antagonism with Zn and its effects on human prostate carcinogenesis were investigated [38, 39]. Another study in rats demonstrated the protective effects of Zn on prostate tissues against Cd toxicity [34] without elucidating the mechanism of this antagonism.

Antagonism between Zn and Cd may be the result of their similar physicochemical properties in many respects. Zn is a competitive antagonist of Cd in living tissues as both Cd and Zn bind to transport proteins and metallothioneins in cells [40–43]. On the other hand, it is known that Zn protects lipid tissues from free radical peroxidation and stabilizes cell membranes [44]. Rogalska et al. showed that Zn supplementation in rats have a protective effect against the toxic symptoms of long-time Cd exposure by preventing lipid peroxidation and hyperlipidemia [45]. Another study showed the preventive effect of Zn treatment on Cd accumulation in the kidneys of rabbits [46]. According to several other literature findings, Zn has the ability to reduce the toxicity of Cd as well as Cd-induced apoptosis and necrosis [47–49].

In this study, the concentration-dependent level of antagonism between Zn and Cd was systematically studied. The antagonism between the two components occurs at different intensities depending on the amounts of these components and is highest in a certain optimum composition [50–53]. In order to determine this optimum Zn-Cd composition, $Zn_{1-x}Cd_xO$ nanoparticles were synthesized in 14 different compositions

in the range of $x=0.00$–0.80. By taking advantage of the antagonistic relationship between Zn and Cd, we aimed to improve the blood compatibility of ZnO while also adjusting the photocatalytic properties of this new material. We investigated the hemolytic potentials of Cd-doped ZnO nanoparticles together with their structural and morphological properties which are directly related to their performances in biomedical area. We believe that our study is going to provide information on this unsearched area of literature and clarify the basic biological properties of $Zn_{1-x}Cd_xO$ nanoparticles for their potential use in biomedical area.

Experimental procedures

Nanoparticle synthesis

$Zn_{1-x}Cd_xO$ ($x=0.00$, 0.01, 0.02, 0.03, 0.04, 0.05, 0.10, 0.20, 0.30, 0.40, 0.50, 0.60, 0.70, and 0.80) polycrystalline nanoparticles were synthesized using sol–gel technique. Zinc acetate dihydrate ($Zn(CH_3COO)_2{\cdot}2H_2O$) and cadmium acetate tetrahydrate ($Cd(CH_3COO)_2.4H_2O$) were used as precursors. Methanol was used as solvent while monoethanolamine was used as sol-stabilizer to prepare clear homogeneous solutions. All reagents were weighed and placed in a pyrex beaker to be used as a reaction vessel, and then mixed with a magnetic stirrer at room temperature until a transparent homogeneous mixture was obtained. To remove the solvent, the lid of the glass beaker was opened, and the solutions were kept under magnetic stirring for 24 h. After removing the solvent, the remaining samples were preheated at 200–350 °C at atmospheric conditions for 10 min. Finally, samples were calcinated in a Box furnace at 600 °C for 10 min to obtain the crystal structure of $Zn_{1-x}Cd_xO$ nanoparticles. Further details on nanoparticle synthesis were given in our previous studies [8, 11].

Structural analysis

The crystalline structures of the $Zn_{1-x}Cd_xO$ nanoparticles were characterized by XRD measurements using a Rigaku diffractometer with CuKα ($\lambda=1.5418$ nm) radiation at room temperature in the scan range of $2\theta=10$–$90°$ with a scan speed of $3°$ min^{-1} and a step increment of 0.02°. The surface morphology of the $Zn_{1-x}Cd_xO$ nanoparticles was established by using SEM (JEOL, JSM-5910LV) and TEM (JEOL JEM-2100).

Photocatalytic activity measurements

$Zn_{1-x}Cd_xO$ ($0.0\leq x\leq 0.8$) nanoparticles were investigated by means of their photocatalytic properties by pursuing the degradation of crystal violet (CV) in aqueous media under 254 nm irradiation. The concentration of aqueous nanoparticle dispersions and CV solution was adjusted as 1.0 mg mL^{-1} and 2.5×10^{-6} M respectively. The photocatalytic activity measurement setup was comprised of a polytetrafluoroethylene-coated magnetic stirring bar and a glass beaker containing 50-mL aqueous solution of CV and the appropriate amount of the photocatalyst ($Zn_{1-x}Cd_xO$). Photoreaction mixtures were brought to surface adsorption–desorption equilibrium in the dark at room temperature under continuous magnetic stirring for 30 min. Then, nanoparticle dispersions were irradiated while being continuously stirred under 254 nm excitation. The irradiation was carried out using a couple of UV lamps (45 W each) which was placed vertically on the reaction vessels at a distance of 40 cm. At specific time intervals, 1.5 mL of aliquots was withdrawn and centrifuged at 4000 rpm for 3 min to settle the suspended nanoparticles down. The absorption spectra of the supernatant was measured using a Shimadzu UV mini 1240 UV/vis spectrophotometer and concentration of the undegraded CV was determined by considering the characteristic absorption maxima at around 591 nm and using the calibration graph drawn for the CV. Distilled water was used as the reference solution for all measurements. Photocatalytic properties of $Zn_{1-x}Cd_xO$ nanoparticles were investigated by following the decolorization percentage of CV via the following equation [54].

$$\text{Decolorization}\ (\%) = ((C_o - C)/C_o)x100 \quad (1)$$

In Eq. 1, C_o and C refer for the concentration of CV before irradiation, and the concentration of CV after a certain irradiation time (t), respectively. The photocatalytic degradation kinetics of CV were studied using the first order kinetics and rate constants for the degradation reactions were determined by Eq. 2 as given by Karthik et al. [24].

$$\ln(A0/A) = k.t \quad (2)$$

In Eq. 2, A_o and A were the absorbance values of the CV solution immediately after the surface

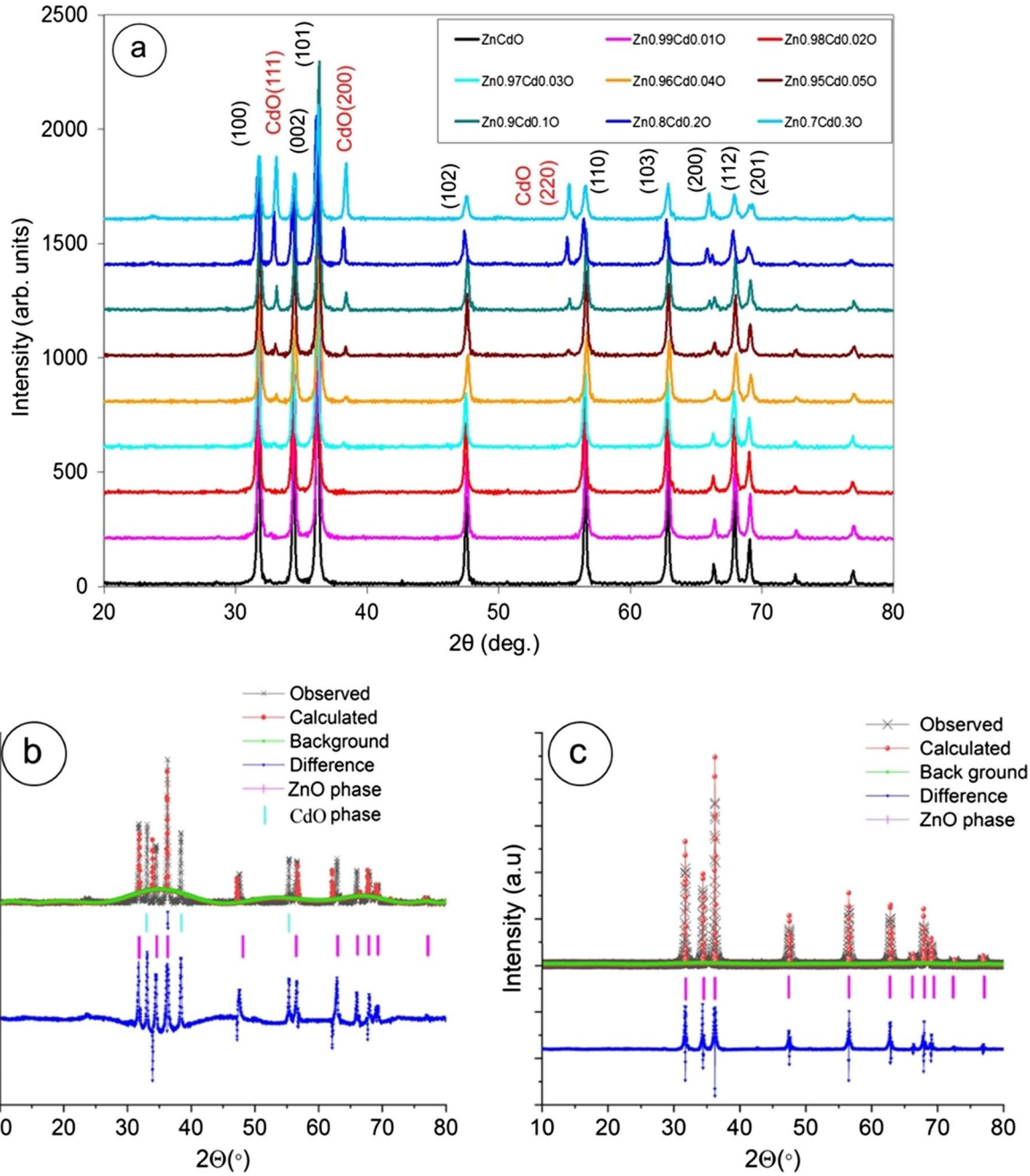

Fig. 1 XRD patterns of $Zn_{1-x}Cd_xO$ ($x = 0.00$, 0.01, 0.02, 0.03, 0.04, 0.05, 0.10, 0.20, 0.30, 0.40, 0.50, 0.60, 0.70, and 0.80) nanoparticles. ZnO planes were shown in black color in **a**, and Rietveld analysis of $Zn_{0.70}Cd_{0.30}O$ and $Zn_{0.99}Cd_{0.01}O$ samples in **b** and **c** respectively

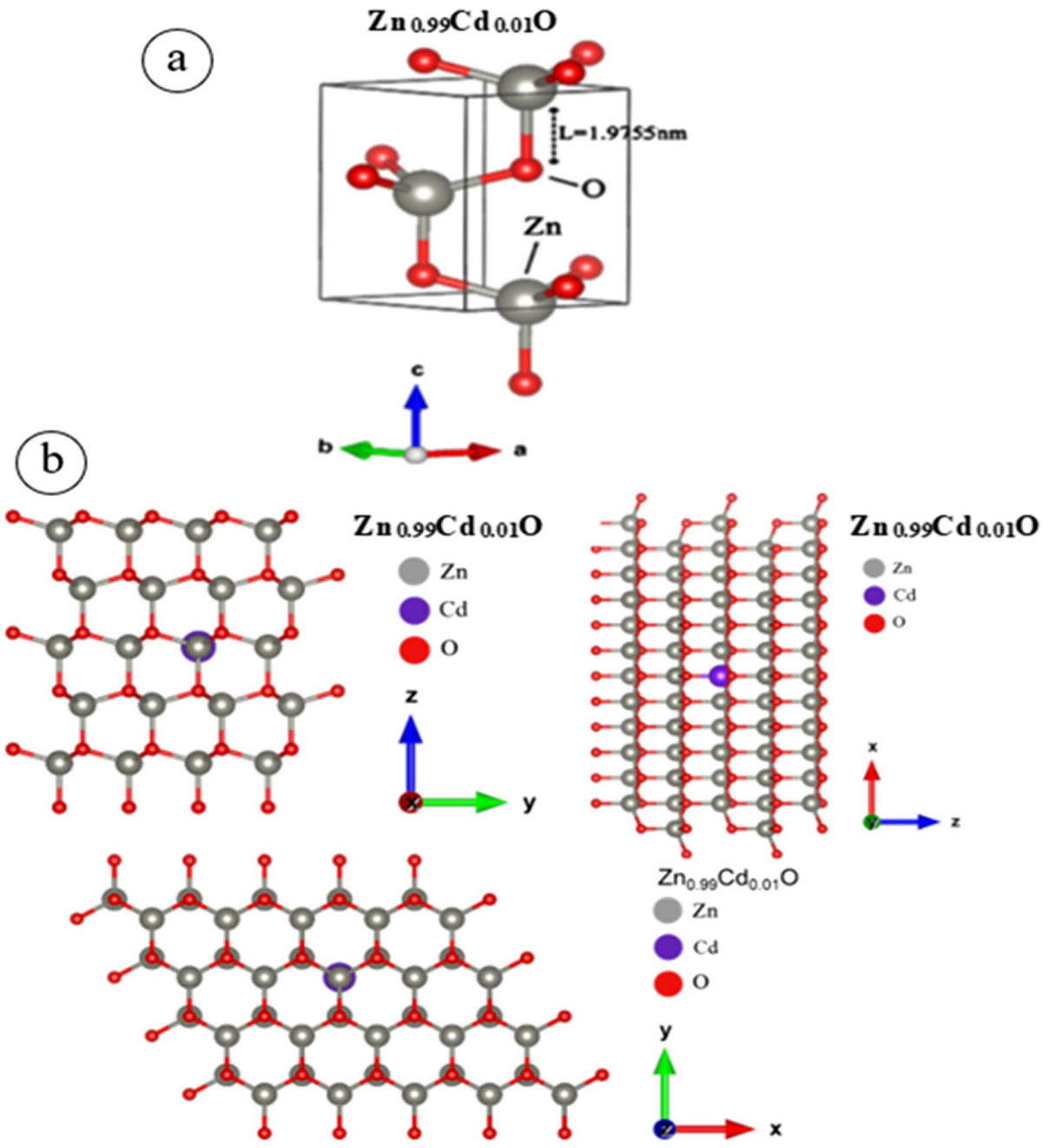

Fig. 2 **a** Representation of a unit cell of $Zn_{0.99}Cd_{0.01}O$ and **b** representation of crystal structure of $Zn_{0.99}Cd_{0.01}O$ nanoparticle using VESTA visualization package

Table 1 Cd concentration-dependent average particle sizes *D*, lattice parameters *a* and *c*, atomic packing factor (*c/a*), and cell volume

Sample	D (nm)	a (Å)	c (Å)	c/a	Cell volume
ZnO	39.636	3.253	5.210	1.6016	47.731
$Zn_{0.99}Cd_{0.01}O$	38.611	3.247	5.198	1.6012	47.450
$Zn_{0.98}Cd_{0.02}O$	35.268	3.255	5.216	1.6025	47.847
$Zn_{0.97}Cd_{0.03}O$	34.193	3.255	5.216	1.6025	47.849
$Zn_{0.96}Cd_{0.04}O$	30.114	3.239	5.187	1.6014	47.117
$Zn_{0.95}Cd_{0.05}O$	38.041	3.245	5.196	1.6013	47.370
$Zn_{0.90}Cd_{0.10}O$	38.418	3.239	5.192	1.6031	47.173
$Zn_{0.80}Cd_{0.20}O$	34.556	3.252	5.204	1.5999	47.682
$Zn_{0.70}Cd_{0.30}O$	28.944	3.251	5.198	1.5991	47.566
$Zn_{0.60}Cd_{0.40}O$	24.203	3.258	5.180	1.5901	47.598
$Zn_{0.50}Cd_{0.50}O$	28.982	3.258	5.179	1.5897	47.594
$Zn_{0.40}Cd_{0.60}O$	27.902	3.258	5.186	1.5917	47.672
$Zn_{0.30}Cd_{0.70}O$	24.707	3.258	5.191	1.5932	47.734

adsorption equilibrium was established for CV and at the end of a given photodegradation time (t), respectively. k was the first order rate constant for the photocatalytic degradation.

Blood compatibility tests

Blood compatibilities of $Zn_{1-x}Cd_xO$ nanoparticles were investigated. Blood samples were drawn from healthy volunteers via a single-use syringe of 5 mL. Blood samples were anticoagulated using the 0.108 mM aqueous solution of trisodium citrate. Blood: trisodium citrate ratio was adjusted as (9:1). Anticoagulated whole blood samples were diluted by phosphate buffer solution (PBS) then centrifuged at 4000 rpm for 5 min to separate the erythrocytes (red blood cells (RBCs)) from blood plasma. After decantation of the supernatant, 50-mL erythrocyte stock-solution was prepared by dilution using PBS. Appropriate amounts from RBC stock solution were mixed with 5.0 mL of $Zn_{1-x}Cd_xO$ nanoparticle suspensions in 1.0 mg mL^{-1} and 5.0 mg mL^{-1} concentrations. Positive and negative control tests were performed by using distilled deionized water (DDW) and phosphate buffer solution, respectively. Positive (100% hemolysis) and negative control (0% hemolysis) tests were performed using distilled water and phosphate buffer solution, respectively. $Zn_{1-x}Cd_xO$ nanoparticle-erythrocyte dispersions were incubated under magnetic stirring at 37 °C for 3 h. All tests were performed in duplicate. Then, samples were centrifuged at 3000 rpm for 5 min and absorbance of supernatant was measured between 200 and 800 nm using a UV–visible spectrophotometer to indicate hemoglobin released into the medium as a result of erythrocyte lysis. Percentage of hemolysis for each $Zn_{1-x}Cd_xO$ composition was calculated based on the absorbance value (ABS) of the supernatant at 540 nm using the equation given below [55].

$$\%Hemolysis = \frac{ABS_{testsample} - ABS_{negativecontrol}}{ABS_{positivesample} - ABS_{negativecontrol}} \quad (3)$$

Table 2 The varying of Cd concentration in ZnO nanoparticles-dependent dislocation density (δ) (the amount of defect in the sample), the locality of the atoms and their displacement (u), bond length (L) and stress (σ), and microstrain (Ɛ)

Sample	δ (nm^{-2})	u	L (Å)	σ*10^9 (N m^{-2})	Ɛ
ZnO	0.00064	0.37994	1.9794	− 23.2108	0.00087453
$Zn_{0.99}Cd_{0.01}O$	0.00067	0.38001	1.9755	− 23.1670	0.00089775
$Zn_{0.98}Cd_{0.02}O$	0.00080	0.37981	1.9809	− 23.2404	0.00098285
$Zn_{0.97}Cd_{0.03}O$	0.00086	0.37980	1.9810	− 23.5088	0.00101375
$Zn_{0.96}Cd_{0.04}O$	0.00110	0.37998	1.9708	− 22.8748	0.00115108
$Zn_{0.95}Cd_{0.05}O$	0.00069	0.38000	1.9744	− 23.1608	0.00091121
$Zn_{0.90}Cd_{0.10}O$	0.00068	0.37970	1.9716	− 23.3689	0.00090228
$Zn_{0.80}Cd_{0.20}O$	0.00084	0.38021	1.9787	− 23.1783	0.00100312
$Zn_{0.70}Cd_{0.30}O$	0.00119	0.38035	1.9771	− 23.1487	0.00119761
$Zn_{0.60}Cd_{0.40}O$	0.00171	0.38184	1.97781	− 22.1448	0.00087453
$Zn_{0.50}Cd_{0.50}O$	0.00119	0.38190	1.97776	− 22.0932	0.00089775
$Zn_{0.40}Cd_{0.60}O$	0.00128	0.38157	1.97877	− 23.3242	0.00098285
$Zn_{0.30}Cd_{0.70}O$	0.00164	0.38133	1.97960	− 23.3798	0.00101375

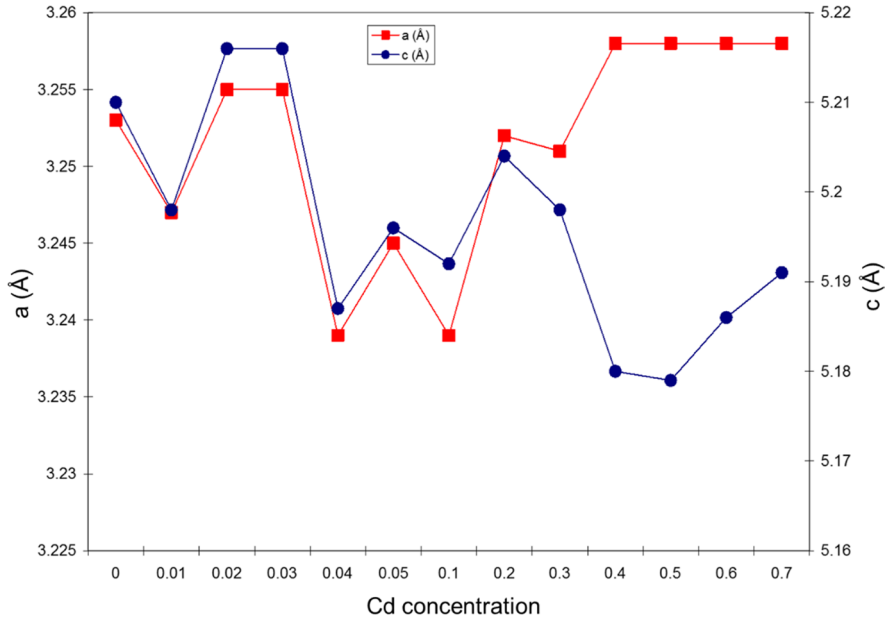

Fig. 3 Cd concentration-dependent lattice parameters a and c for $Zn_{1-x}Cd_xO$ nanoparticles

Results and discussions

Structural properties

Synthesis conditions affect the structural, electrical, magnetic, photocatalytic, and hemolytic properties of the obtained $Zn_{1-x}Cd_xO$ nanoparticles. XRD applying the Rietveld refinement method was performed in the range of $10° \leq 2\theta \leq 80°$ in order to display the crystal structure properties and the existing phases of $Zn_{1-x}Cd_xO$ nanoparticles. The XRD patterns of $Zn_{1-x}Cd_xO$ $(0.0 \leq x \leq 0.8)$ nanoparticles are shown in Fig. 1a. The XRD patterns showed all characteristic peaks of ZnO lattice indicating the presence of a hexagonal structure (space group P63mc), and patterns were also in agreement with standard JCPDS files (Card no. 36–1451). In Fig. 1a, planes for ZnO and CdO phases were shown in black and red color,

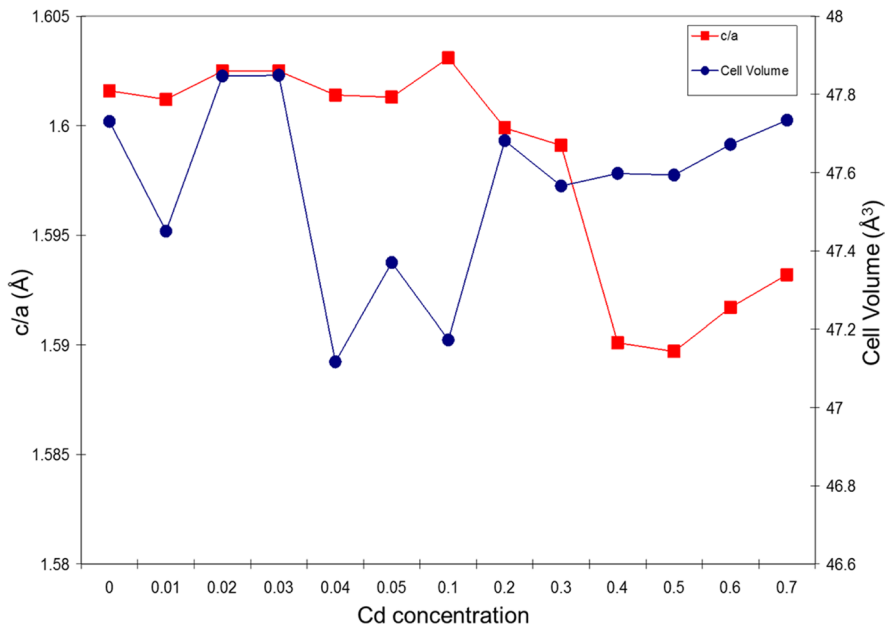

Fig. 4 Cd concentration-dependent c/a and cell volume for $Zn_{1-x}Cd_xO$ nanoparticles

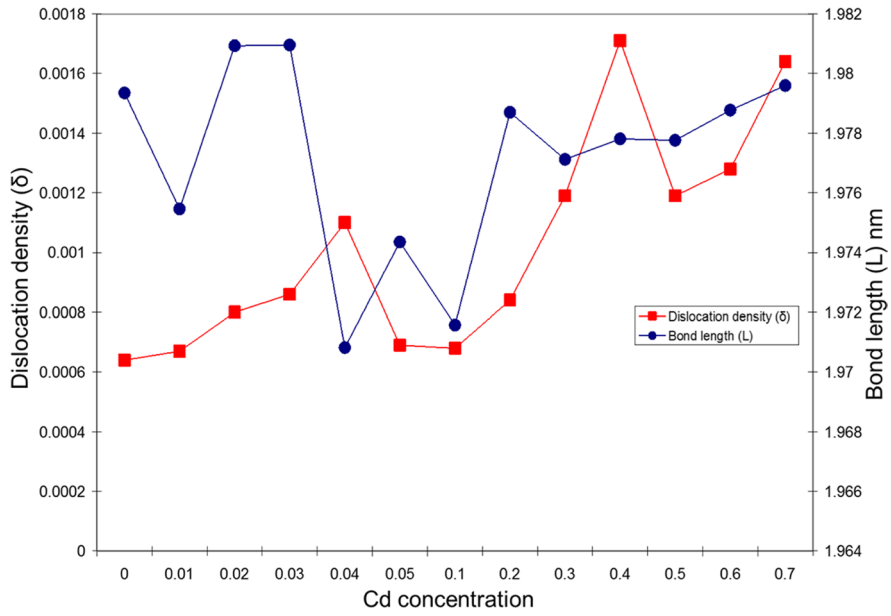

Fig. 5 Cd concentration-dependent dislocation density and bond length for $Zn_{1-x}Cd_xO$ nanoparticles

respectively. CdO has the cubic structure with the space group $Fm\bar{3}m$. These results are compatible with the literature [56, 57]. The ionic radius of Cd^{2+} (0.97 Å) is larger compared to Zn^{2+} (0.74 Å). Up to $x \leq 0.2$, Cd replaces Zn and ZnO yields single phase, for $x > 0.2$, two phases are formed as it is partially displaced; ZnO and CdO.

The important points emphasized by the studies presented in the literature are that the structural properties of metal oxide nanoparticles may change depending on parameters such as the synthesis method applied, the solvents used, and the type of precursor, whether calcination is applied or not and the calcination temperature [58–60]. Although some literature studies have reported that ZnCdO binary nanoparticles synthesized in various compositions do not show characteristic peaks of the CdO phase in addition to the ZnO phase, some other studies prove the presence of CdO in the nanoparticle structure by XRD patterns. For example, it has been reported that the $Zn_{1-x}Cd_xO$ ($0.0 \leq x \leq 0.8$)

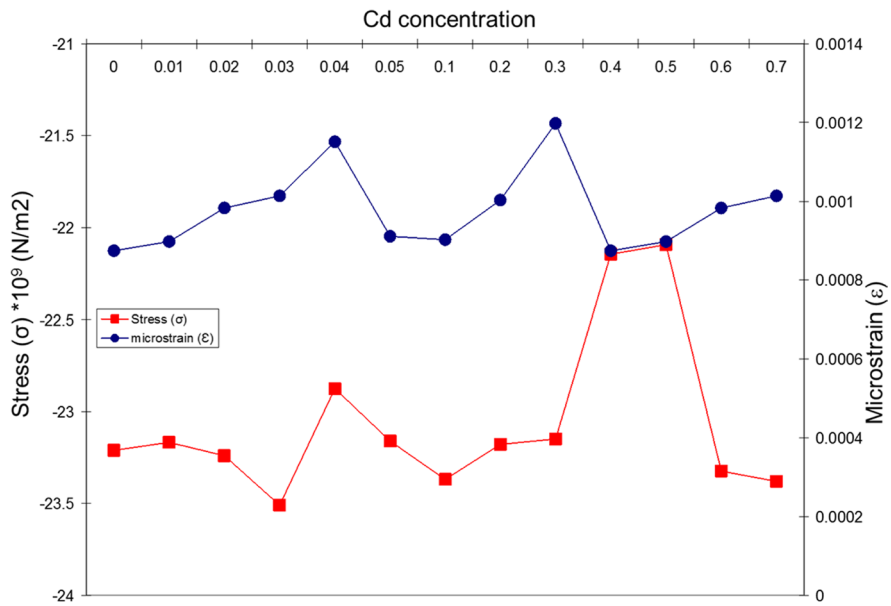

Fig. 6 Cd concentration-dependent stress and microstructure for $Zn_{1-x}Cd_xO$ nanoparticles

nanoparticles which their precursors were dissolved in ethylene glycol and prepared by applying an additional microwave procedure did not show peaks of an additional CdO phase [61]. In some other studies, the CdO phase occurring in the metaloxide structure and appeared in the (220) plane was observed at low Cd doping rates. Results were compatible with the XRD findings obtained from this study [62, 63].

As seen in Fig. 1a, a single ZnO phase with a Cd doping ratio up to $x<0.04$ was obtained. After this doping ratio, both ZnO and CdO phases were obtained. A more comprehensive research was conducted with Rietveld analysis and the results obtained were compared. According to the Rietveld analysis results, Cd-doped samples up to $x<0.03$ concentration was exhibited ZnO phase without any secondary phase in Fig. 1c. However, samples with doping concentration of $x=0.03$ and higher were exhibited both ZnO and CdO phases as shown in Fig. 1b. We conclude that up to $x=0.03$ concentration, there is a single phase, and all patterns match with the hexagonal ZnO lattice. This is because of the larger ionic radius of Cd (ionic radius 0.97 Å) compared to Zn (ionic radius 0.74 Å). Cd replaces Zn one to one until $x<0.03$ contribution ratio, after this doping ratio, Cd does not replace one to one Zn.

The unit cells and crystal structure of $Zn_{0.99}Cd_{0.01}O$ nanoparticles are shown in Fig. 2a and b, respectively. The hexagonal ZnO unit cell (Fig. 2a) and the random 1% Cd-doped ZnO crystal structure (Fig. 2b) were visualized with the VESTA visualization package using the experimentally obtained parameters which are depicted in Tables 1 and 2.

The concentration-dependent particle sizes (D), lattice parameters (a and c), and atomic packing factor (c/a), cell volume, dislocation density (δ) (the amount of defect in the sample), the locality of the atoms and their displacement (u), bond length (L) microstrain (Ɛ), and stress (σ) are evaluated and depicted in Tables 1 and 2 using XRD analysis of Cd-doped

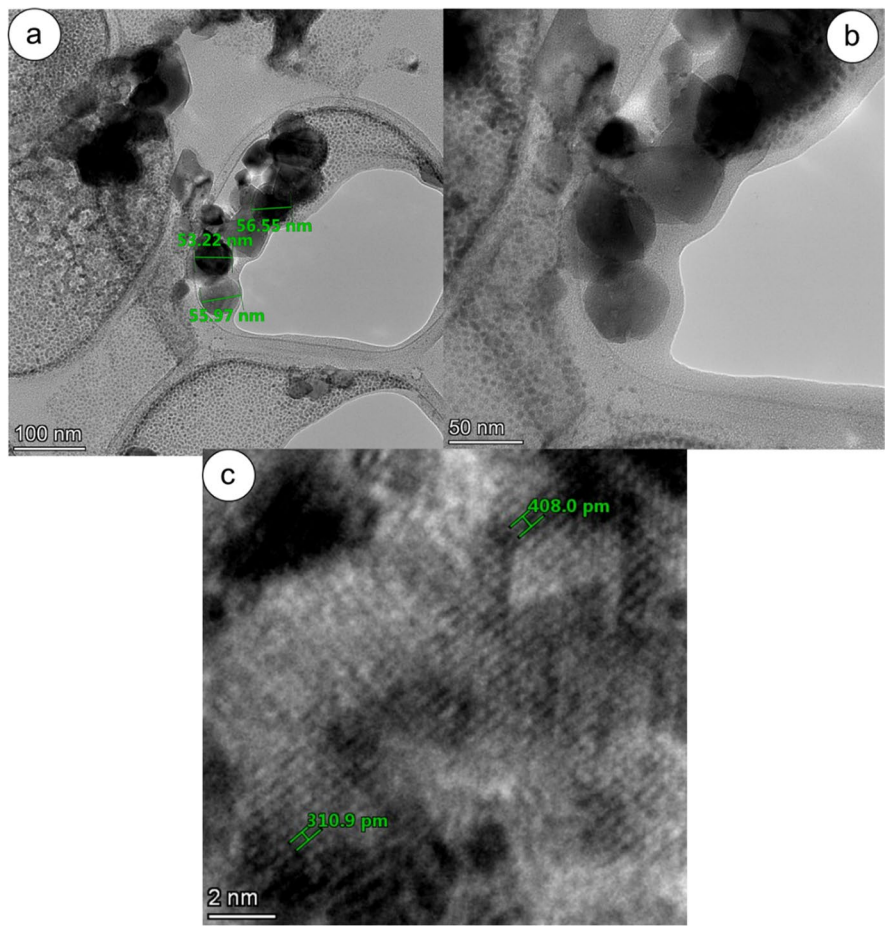

Fig. 7 **a–c** TEM images of $Zn_{0.40}Cd_{0.60}O$ nanoparticles under different magnifications

ZnO nanoparticles. The detailed evaluations of these parameters can be found in references [8, 11]. Particle sizes (D) are affected by annealing procedure. During annealing, the sizes of grains increase and inter-grain bindings occur. It has also been reported that the grain size increases significantly after annealing process. In this study, the decrease in particle sizes could be attributed to the increasing number of Cd atoms exerting drag forces on boundary motion, hence having effect on grain growth. Additionally, decreasing crystallite size of ZnO with increasing amount of Cd ions also reveals that Cd in ZnO matrices creates a compressive strain. Similar results have been reported in the literature in different studies on CdZnO containing varying amounts of Cd [64–66].

The lattice parameters a and c of $Zn_{1-x}Cd_xO$ nanoparticles were in the range of 3.239–3.258 Å and 5.179–5.216 Å, respectively, as shown in Fig. 3 and Tables 1 and 2. The c/a value in Fig. 4 drops sharply after the Cd concentration $x > 0.3$ from the c/a = 1.60 value in the literature. This is because, as seen in Fig. 1, after Cd concentration $x > 0.3$, the CdO cubic structure becomes dominant. Therefore, when XRD patterns were examined after Cd concentration $x > 0.3$ as shown in Fig. 1, it was observed that nanoparticles are cubic Fm-3 m CdO crystal structure.

It is seen in Fig. 5 that the dislocation density increases with increasing Cd concentration. In other words, it shows the change in the amount of defect. The Zn-O bond lengths (L), which fluctuate up to $x < 0.2$ Cd concentration, almost do not change after this concentration value.

The negative signs of stress values show compressive stresses as seen in Table 2 and Fig. 6. Stress values are seen to fluctuate between 22.0932 and 23.5088 N m^{-2}. In addition, microstrain values change between

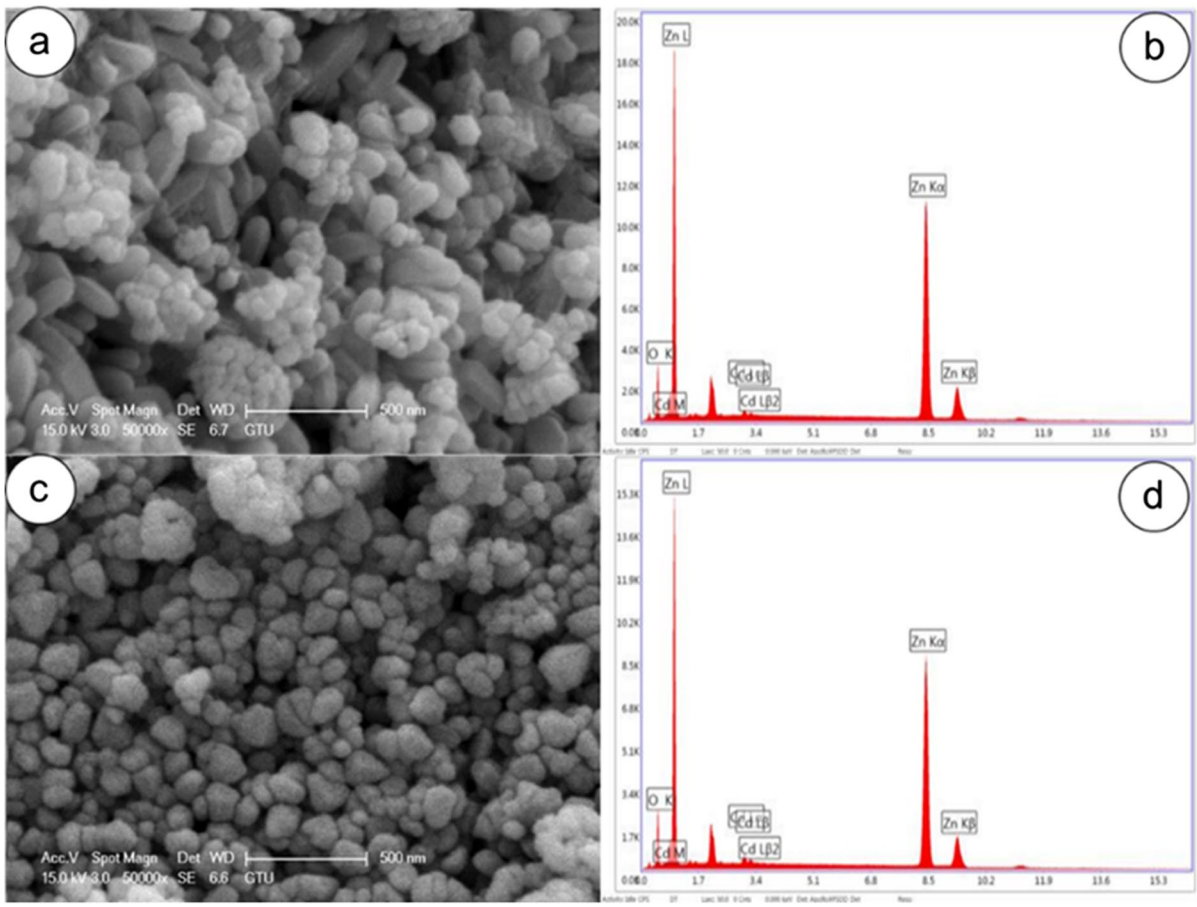

Fig. 8 SEM micrographs and EDX results of $Zn_{0.98}Cd_{0.02}O$ ((**a**) and (**b**), respectively) and $Zn_{0.97}Cd_{0.03}O$ ((**c**) and (**d**), respectively)

0.00087453 and 0.00119761. The fluctuations in microstrain and stress values indicate the variation of physical defects and dislocations in the host lattice structure.

The morphology characteristics of ZnCdO nanoparticles

The morphology and elemental concentration of all $Zn_{1-x}Cd_xO$ nanoparticles was studied by SEM, TEM, and EDX, respectively. Figure 7a–c shows the TEM image of the $Zn_{0.40}Cd_{0.60}O$ NPs with different scales ranging from 2 to 100 nm. From the SEM micrographs as seen in Figs. 8, 9, 10, and 11, the particle distributions in the range 500 nm magnifications were dense, quasi-spherical, and agglomerating. It is seen that the nanoparticles produced by the sol-gel method show crystalline character according to the TEM results (Fig. 7c). This result agrees with the sharp XRD lines in Fig. 1. Also, as observed from Fig. 7c, the atomic planes appear to be clearly aligned along the micrograph, which is the result of the nanoparticles being crystalline. The interplanetary distance is approximately 308–408 pm. The nanoparticle sizes from the TEM results are 53–56.55 nm. The mismatch with the calculated values is due to agglomeration. The elemental compositions of $Zn_{1-x}Cd_xO$ nanoparticles were provided by EDX analysis exhibited in Figs. 8b–d, 9b–d, 10b–d, and 11b. Only the Zn and Cd peaks were seen on the EDX graph, without any unwanted extra elemental peak contributions.

Blood compatibilities

Materials designed to be used for biological applications must be well defined in respect to their biocompatibility. Blood compatibility measurements are

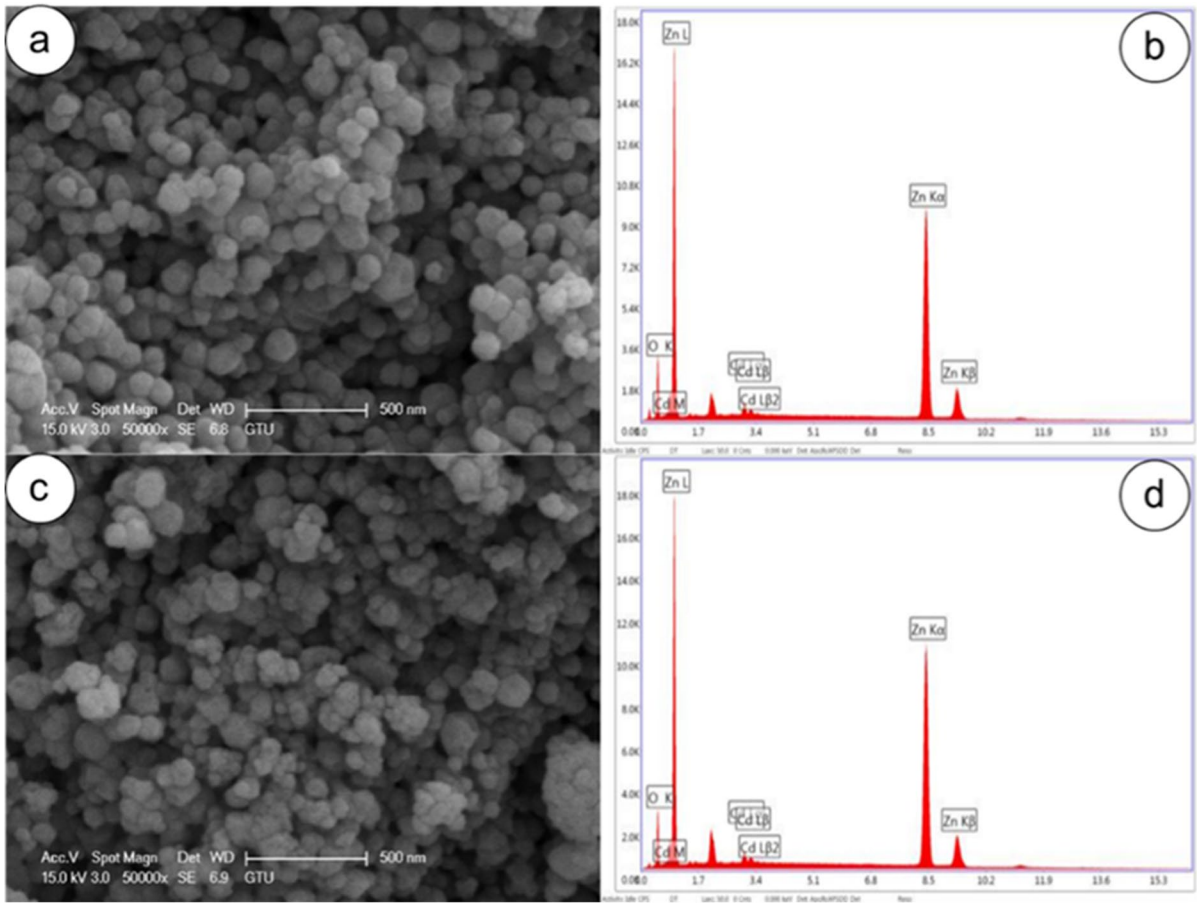

Fig. 9 SEM micrographs and EDX results of $Zn_{0.96}Cd_{0.04}O$ ((**a**) and (**b**), respectively) and $Zn_{0.95}Cd_{0.05}O$ ((**c**) and (**d**), respectively)

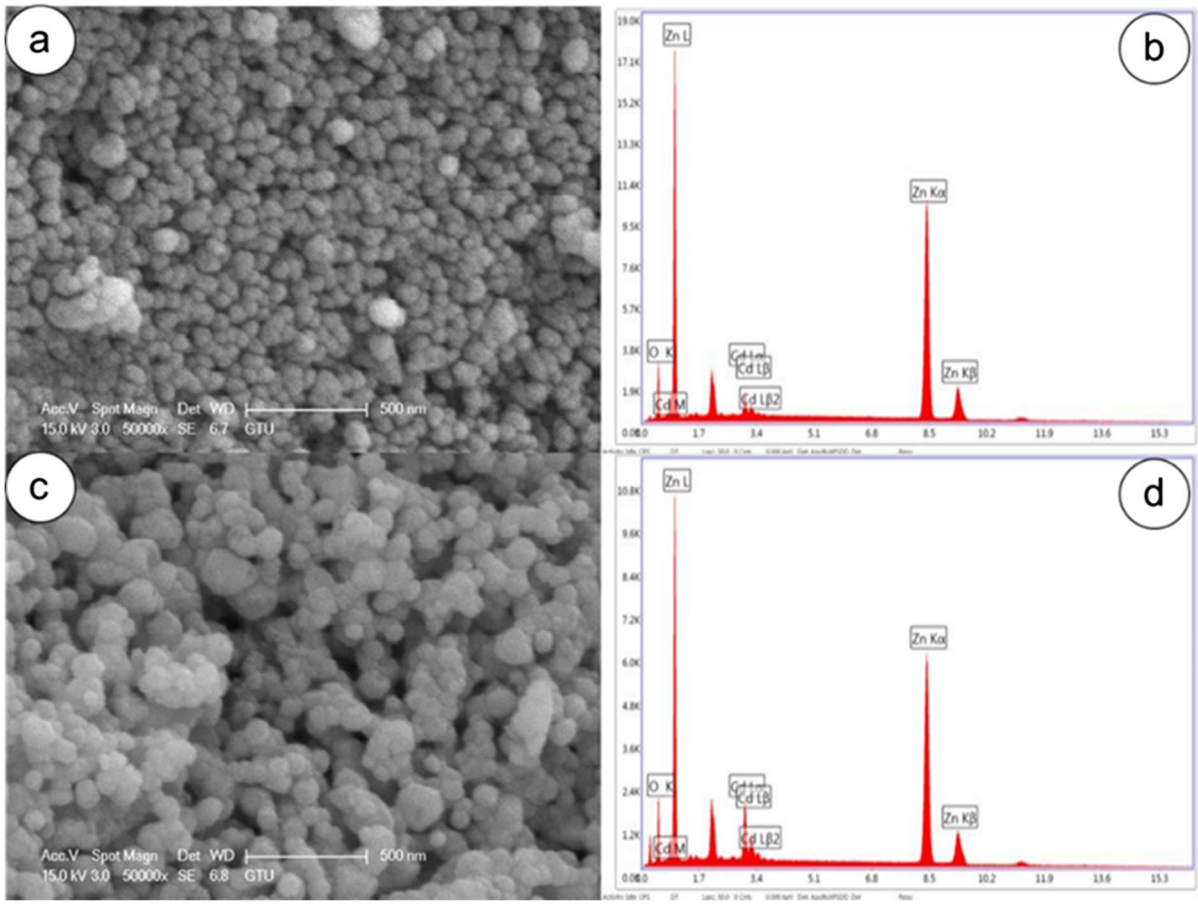

Fig. 10 SEM micrographs and EDX results of $Zn_{0.90}Cd_{0.10}O$ ((**a**) and (**b**), respectively) and $Zn_{0.80}Cd_{0.20}O$ ((**c**) and (**d**), respectively)

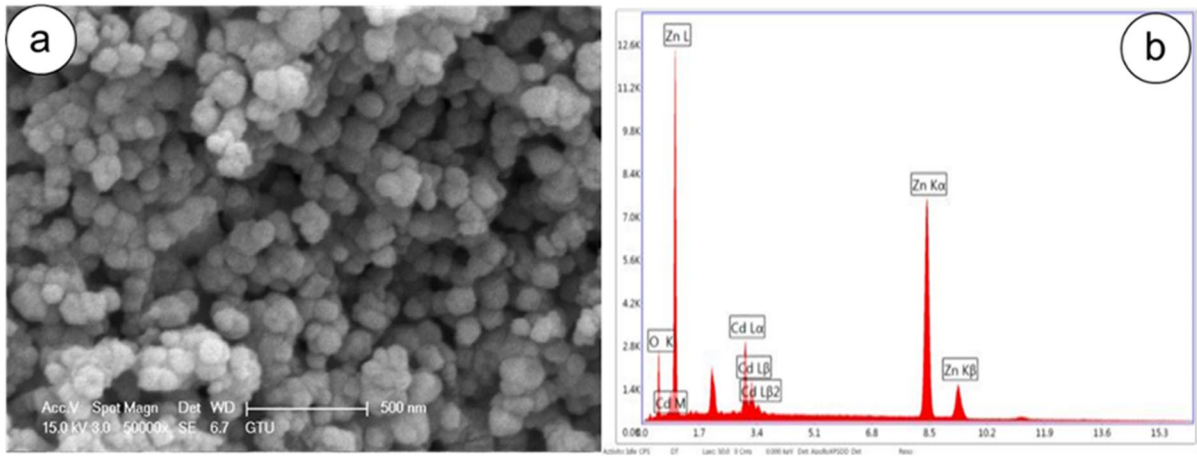

Fig. 11 SEM micrographs of $Zn_{0.70}Cd_{0.30}O$ nanoparticles for 500 nm in **a**; the EDX graphs of $Zn_{0.70}Cd_{0.30}O$ nanoparticles in **b**

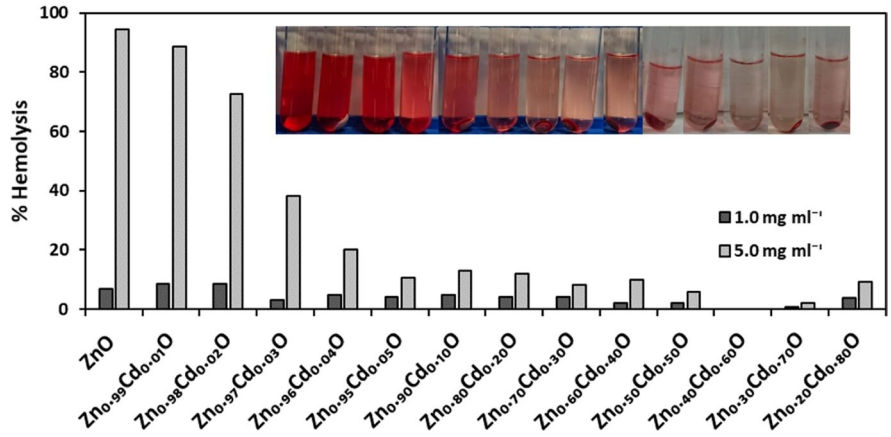

Fig. 12 Hemolysis percentages of RBCs after incubation with $Zn_{1-x}Cd_xO$ nanoparticles. Inset shows the after-incubation images of test samples in the given order of graphic

well accepted tests for the assessment of the biocompatibility between a synthetic material and living tissues [67, 68]. Synthetic nano-sized materials affect the structure of the erythrocyte membrane, alter their physiological functions, and cause lysis [69]. Nanoparticle-induced hemolysis may be reduced by adjusting the hemotoxicity of these synthetic materials.

In this study, human erythrocytes were exposed to two different concentrations (1.0 mg mL^{-1} and 5.0 mg mL^{-1}) of $Zn_{1-x}Cd_xO$ nanoparticles and nanoparticle-induced hemolysis ratios were determined (Fig. 12). While positive control test refers to RBCs stimulated with PBS, negative control refers to RBCs only stimulated with distilled water. In the presence of RBCs in water (positive control test), the osmotic imbalance makes water move into the RBCs, swells them, and causes the cell membrane to burst and the cell contents to leak out. On the contrary, PBS provides a hypotonic environment for RBCs and inhibits cell lysis. According to the experimental results, erythrocytes subjected to 3 h of incubation at 37 °C were slightly lysed in different percentages by the effect of nanoparticles at 1.0 mg mL^{-1} concentration. While hemolysis ratios were 8.4% for both $Zn_{0.99}Cd_{0.01}O$ and $Zn_{0.98}Cd_{0.02}O$, hemolytic effect of nanoparticles was gradually decreased with increasing Cd doping ratio. This downward tendency was observed in grain sizes for samples from ZnO to $Zn_{0.96}Cd_{0.04}O$ and from $Zn_{0.95}Cd_{0.05}O$ to $Zn_{0.70}Cd_{0.30}O$. Strong hemolytic activity of ZnO was decreased and reached relatively low ratios and finally to the zero point at an optimum Cd doping

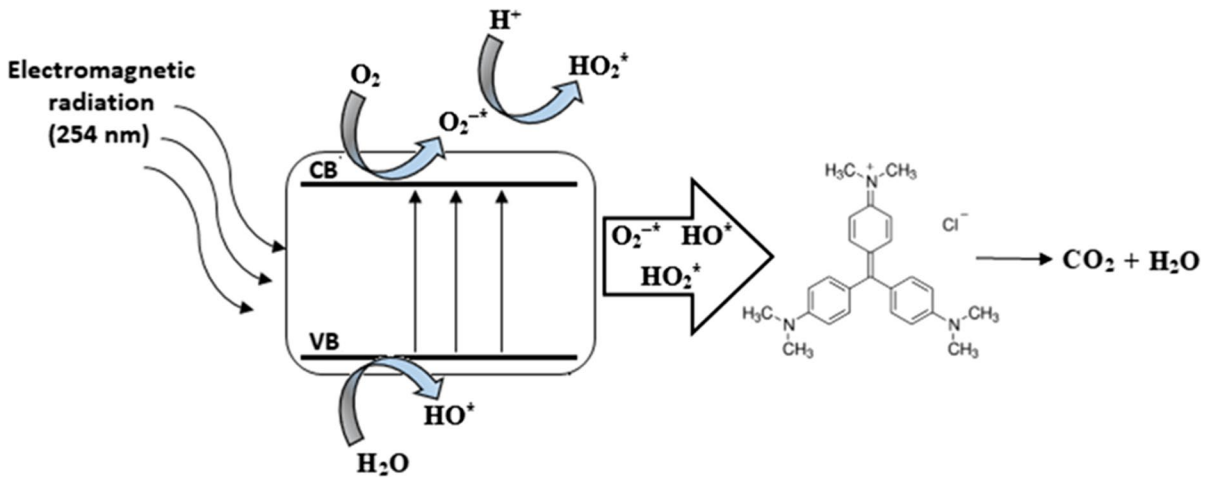

Fig. 13 Schematic representation for the photodegradation of CV

Table 3 Photocatalytic degradation rate constants and CV removal efficiencies for ZnO and $Zn_{1-x}Cd_xO$ nanoparticles

Samples	Degradation rate constants k (min^{-1})	CV degradation (%)
ZnO	0.0012	36.9
$Zn_{0.99}Cd_{0.01}O$	0.0022	56.4
$Zn_{0.98}Cd_{0.02}O$	0.0011	36.8
$Zn_{0.97}Cd_{0.03}O$	0.0017	47.7
$Zn_{0.96}Cd_{0.04}O$	0.0016	44.7
$Zn_{0.95}Cd_{0.05}O$	0.0022	53.9
$Zn_{0.90}Cd_{0.10}O$	0.0031	69.9
$Zn_{0.80}Cd_{0.20}O$	0.0033	72.8
$Zn_{0.70}Cd_{0.30}O$	0.0019	50.5
$Zn_{0.60}Cd_{0.40}O$	0.0018	47.1
$Zn_{0.50}Cd_{0.50}O$	0.0015	42.6
$Zn_{0.40}Cd_{0.60}O$	0.0010	32.2
$Zn_{0.30}Cd_{0.70}O$	0.0014	35.8
$Zn_{0.20}Cd_{0.80}O$	0.0015	37.7

ratio of $x=0.60$. Any lysis in human erythrocytes was not observed at both 0.01 mg mL^{-1} and 5.0 mg mL^{-1} concentrations of $Zn_{0.40}Cd_{0.60}O$. This impressive finding of hemocompatibility could be attributed specifically to the presence of an antagonistic interaction of Zn and Cd. The toxic effect of a mixture on living things may be stronger (antagonism) or weaker (synergism) than the sum of the individual toxic effects of each component forming the mixture. In a study examining the genotoxic effects of Zn and Cd on Carassius gibelio B with the erythrocyte micronucleus assay, subjects were exposed to Cd, Zn, and Cd-Zn mixtures (40 mg/L for each). In the study, Cd-Zn antagonism and the resulting low genotoxic effects were emphasized [70]. As for being an essential trace element for living organisms, zinc plays a key role on the activity of more than 300 enzymes, modulates protein synthesis, and affects cell division and proliferation [71]. Zn helps to prevent cell lysis through activation of the oxidant defense system. Increasing lipid peroxidation in Zn deficiency can be ameliorated by Zn supplementation [72]. On the other hand, high chemical affinity of Cd for sulfhydryl (SH) groups and binding ability of -SH containing biomolecules such as cystine and its oxidized dimer cysteine lead the formation of mercaptaides. Animal experiments rendering direct and indirect evidence of acute and chronic Cd exposure prove that Cd-induced formation of ROS (superoxide anion, hydroxyl radicals, and hydrogen peroxide) causes deleterious health effects. Although numerous toxic effects of Cd on biological systems have been noted, it has been proved that Cd-Zn coexistence has a significant preventive effect on the rat tissues for Cd exposure [73].

According to our results given in Fig. 12, $Zn_{1-x}Cd_xO$ nanoparticles show hemolysis ratios less than 5% indicating low in vitro toxicity and negligible hemolytic activity at 1.0 mg mL^{-1} for Cd doping ratios higher than 0.02. Hemolysis ratios which are less than 5% are regarded as safe by the standard test method for the analysis of hemolytic products of nanoparticles (ASTM E2524-08). At a critical Cd doping ratio ($x=0.60$), hemolysis reached a minimum of 0% and the proposed material became a completely hemocompatible nature. At $x=0.60$ ratio, the amount of Cd in the ZnO matrix reached a critical concentration, and the antagonism between Zn and Cd elements was weakened with further increase in Cd concentration.

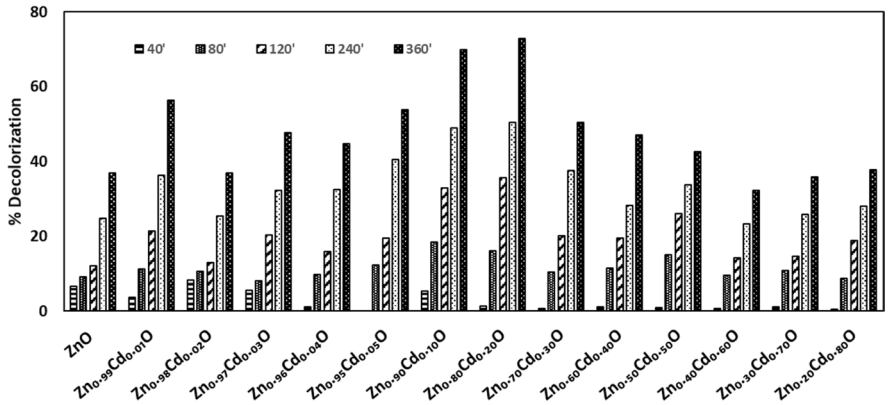

Fig. 14 Decolorization profiles of ZnO and $Zn_{1-x}Cd_xO$ nanoparticles

Photocatalytic properties

Electron transfers between valence- and conduction-band of semiconductors form electron-hole pairs lead to the formation of ROS which are assumed to be responsible from the intracellular oxidant stress, chronic inflammatory diseases, tumors, and cell death [74–76].

ROS formation from metal oxide nanoparticles is a well-defined oxidative process comprised of three major steps. The first step is the excitation of valence band (VB) electrons by the electromagnetic radiation having energy higher than the band gap of metal oxide (Eq. 4). Excited electrons migrate to the conduction band (CB) leaving an equal number of electron holes in VB. Simultaneously, excited electrons move to the surface to initiate degradation reactions. In the last step, the photogenerated electron–hole pairs taking part in redox reactions result in the formation of ROS such as hydroxyl radicals (OH^*), hydroperoxyl radicals (HO_2^*), superoxide radicals (O_2^{-*}), and H_2O_2.

Photogenerated electrons interact with O_2 to form oxygen anion radicals (O_2^{-*}) (Eq. 5), electron holes in the VB react with H_2O molecules to produce hydroxyl radicals (HO^*) (Eq. 6). This reaction series goes on further as to produce other radicalic species (HO^*, HO_2^*) (Eqs. 7 and 8) possessing sufficient energy for the photocatalytic degradation of CV (Eq. 9).

$$Zn_{1-x}Cd_xO + hv \rightarrow Zn_{1-x}Cd_xO + e^-{}_{(CB)} + h^+{}_{(VB)} \quad (4)$$

$$Zn_{1-x}Cd_xO\ e^-{}_{(CB)} + O_2 \rightarrow Zn_{1-x}Cd_xO + O_2^{-*} \quad (5)$$

$$H_2O + h^+{}_{VB} \rightarrow H^+ + HO^* \quad (6)$$

$$O_2{}^{-*} + H^+ \rightarrow HO_2{}^* \rightarrow\rightarrow H_2O_2 + O_2 \quad (7)$$

$$H_2O_2 + O_2{}^{-*} \rightarrow HO^* + OH^- + O_2 \quad (8)$$

$$O_2^{-*}, HO^*, HO_2{}^* + CV \rightarrow \text{degradationproductsofCV}\left(CO_2 \text{and} H_2O\right) \quad (9)$$

In this study, $Zn_{1-x}Cd_xO$ nanoparticles were subjected to 254 nm electromagnetic irradiation and the photodegradation of CV was considered evidence of ROS formation by $Zn_{1-x}Cd_xO$ nanoparticles. The schematic representation for the photodegradation of CV is shown in Fig. 13.

Photocatalytic degradation rate constants and time dependent CV decolorization in the presence of pure ZnO and Cd-doped ZnO nanoparticles are given in Table 3 and Fig. 14 respectively. Decolorization percentages were calculated by following the change in the absorbance intensities of CV at 591 nm between 0 and 360 min interval. Results showed that 20% Cd-doped ZnO nanoparticles ($Zn_{0.80}Cd_{0.20}O$) exhibited a maximum decolorization compared to other doping concentrations. This result was attributed to the probable defects and

Table 4 Comparison of ZnO and $Zn_{1-x}Cd_xO$ nanoparticles synthesized by different methods reported in the literature

Nanostructure	Synthesis method	Dye degradation (%) and degradation rate constant		Light source	Reference
ZnO	Thermal decomposition	65 (MB)	50 (RhB)	365 nm of UV light	[80]
$ZnCdC_2O_4$	Thermal decomposition	100 (MB)	100 (RhB)		
CdZnO	Sol–gel method	61 (MB) k:0.008 min^{-1}	–	Visible light	[81]
ZnO	Hydrothermal method	69 (MB) k:0.0293 min^{-1}	–	Sun light	[82]
CdZnO (Cd:4 wt%)	Hydrothermal method	84 (MB) k:0.0619 min^{-1}	–		
$Cd_{0.03}Zn_{0.97}O$	Sol–gel method	91 (MB)	89 (RhB)	Visible light	[83]
ZnO	Sonochemical method	28 (MB) k:0.0012 min^{-1}	24 (MO) k:0.0011 min^{-1}	UV light	[84]
$Cd_{0.03}Zn_{0.97}O$	Sonochemical method	65 (MB) k:0.0029 min^{-1}	45 (MO) k:0.0019 min^{-1}	UV light	
ZnO	Precipitation method	k:0.0012 min^{-1}	–	UV light	[85]
$Cd_{0.03}Zn_{0.97}O$	Precipitation method	89 (MB) k:0.0105 min^{-1}	–	UV light	
$Cd_{0.10}Zn_{0.90}O$	Hydrothermal method	62 (RhB)	–	311 nm of UV light	[86]

MB, methylene blue; *MO*, methyl orange; *RhB*, rhodamine B

oxygen vacancies created by the incorporation of Cd ions into the ZnO matrix [77].

The kinetics of the degradation reaction of CV was investigated by using the logarithm of the relative concentration of the model dye in the solution ($\ln(A_0/A)$) and the irradiation time (t) (Eq. 2). Photocatalytic degradation rate constants of ZnO and $Zn_{1-x}Cd_xO$ nanoparticles are listed in Table 3. The degradation rate constant of ZnO was calculated as 0.0012 min^{-1} while the corresponding values of Cd-doped ZnO samples were in the range of 0.0010–0.0033 min^{-1}. The highest and lowest k values were found as 0.0033 min^{-1} and 0.0010 min^{-1} for $Zn_{0.80}Cd_{0.20}O$ and $Zn_{0.40}Cd_{0.60}O$ respectively. Results were coherent with the percent degradation values of CV. Moreover, it was observed that $Zn_{0.40}Cd_{0.60}O$ nanoparticles which have the lowest photocatalytic activity among all the samples also have the highest blood compatibility as expected (Fig. 12). This finding was consistent with the fact that hemolysis could be triggered by ROS generated by nano-sized materials [78, 79]. For comparison, further detailed information from literature work about photocatalytic activity of Cd-doped ZnO nanostructures are listed in Table 4.

Figure 15 shows UV–vis spectra and first-order degradation kinetics of CV in the presence of ZnO, $Zn_{0.90}Cd_{0.10}O$, and $Zn_{0.40}Cd_{0.60}O$ nanoparticles. Photodegradation kinetics were followed the first-order kinetics for all samples. Decreasing band intensities at 591 nm proved the degradation of CV by both ZnO and $Zn_{1-x}Cd_xO$ nanoparticles. Cd-doped ZnO nanoparticles, especially $Zn_{0.90}Cd_{0.10}O$ and $Zn_{0.80}Cd_{0.20}O$, showed significant CV photo-degradation under

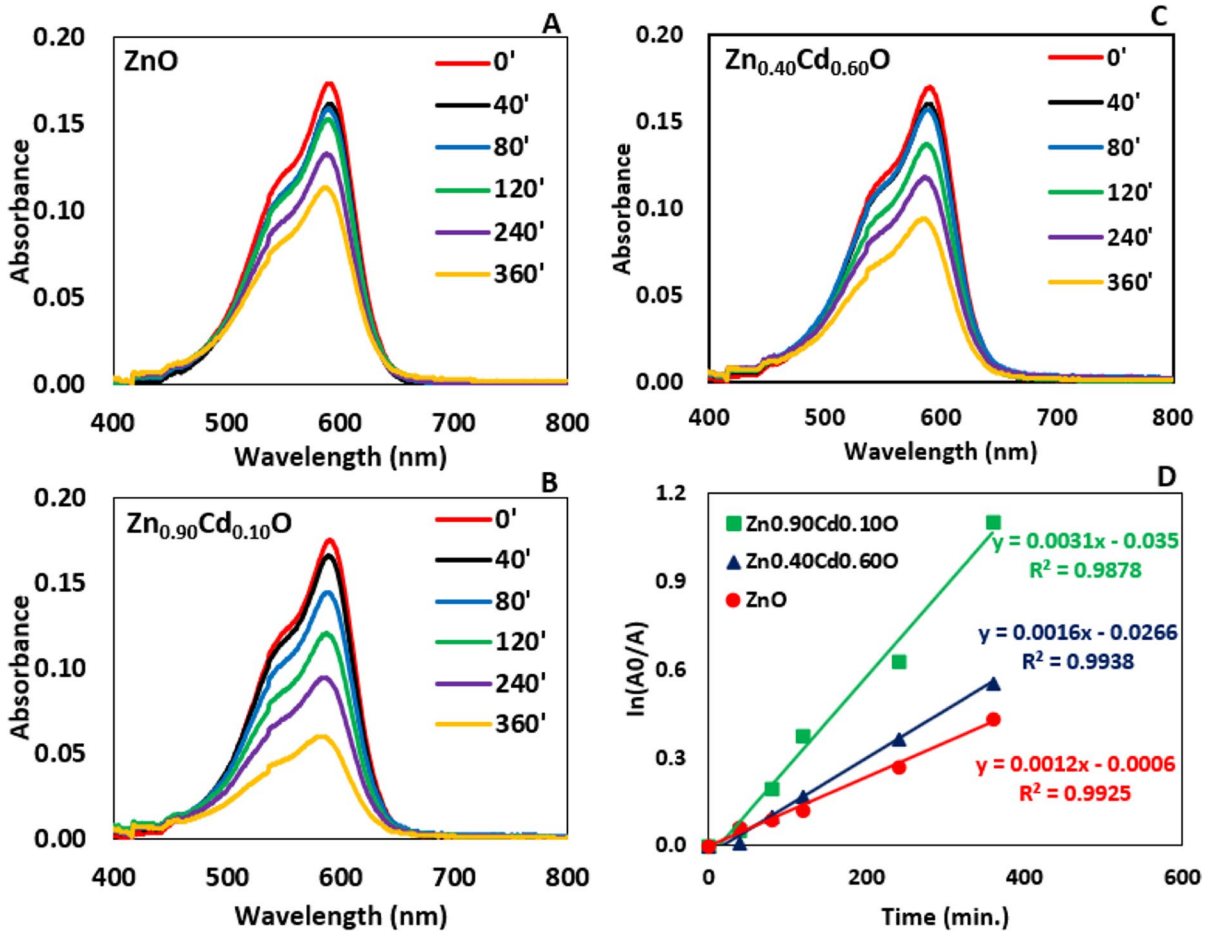

Fig. 15 UV–vis spectra of CV as a function of time for **a** ZnO, **b** $Zn_{0.90}Cd_{0.10}O$, and **c** $Zn_{0.40}Cd_{0.60}O$ under 254 nm irradiation, **d** first-order degradation kinetics of CV for ZnO, $Zn_{0.90}Cd_{0.10}O$, and $Zn_{0.40}Cd_{0.60}O$

the effect of 254 nm irradiation. These samples ($Zn_{0.90}Cd_{0.10}O$ and $Zn_{0.80}Cd_{0.20}O$) with decolorization percentages of 69.9% and 72.8%, respectively, can be proposed as suitable catalysts to be used in wastewater treatment. It can be concluded that the photocatalytic properties of ZnO were enhanced by introducing the varying amounts of Cd into the matrix.

Conclusion

$Zn_{1-x}Cd_xO$ nanoparticles synthesized by the sol-gel method were investigated in terms of their structural, morphological, and photocatalytic properties depending on their chemical composition. Rietveld analysis showed that up to $x < 0.03$, Cd replaces Zn substitutionally yielding ZnO single phase, while for $x \geq 0.03$, two phases are formed, ZnO and CdO. It was seen from SEM micrographs that the distribution of nanoparticles was dense, quasi-spherical, and agglomerating. Photocatalytic properties of Cd-doped ZnO nanoparticles showed that all the samples followed the first-order kinetics photodegradation kinetics under the experimental conditions applied in this study. It was determined that $Zn_{0.80}Cd_{0.20}O$ nanoparticles, which show the highest photocatalytic activity, provide CV photodegradation at a rate of 72.8%. $Zn_{1-x}Cd_xO$ nanoparticles showed undesirable hemolytic effect at low Cd doping ratios for both concentrations. However, the increased concentration of Cd in the ZnO matrix resulted in high hemocompatibility values thought to be due to the antagonistic effect between Cd and Zn. In particular, $Zn_{0.40}Cd_{0.60}O$ nanoparticles showed 0% hemolytic activity at both concentrations. Another promising nanoparticle sample was determined as $Zn_{0.30}Cd_{0.70}O$ having 0.8% and 2.1% hemolysis ratios at 1.0 mg mL^{-1} and 5.0 mg mL^{-1} concentrations respectively.

It is quite unusual to use Cd and Zn-Cd antagonism in order to increase the biocompatibility of ZnO which is very suitable for biomedical applications in terms of material properties. However, the obtained systematic and consistent experimental results show that the antagonistic relationship between Zn-Cd significantly improves the blood compatibility properties of the ZnO matrix in particular. An optimum concentration for Cd-doped nano-sized ZnO ($Zn_{0.40}Cd_{0.60}O$) was obtained, which does not show any detrimental effect on blood biochemistry such as binding with -SH groups or forming methemoglobin but has proven to be potentially effective in the degradation of CV. It is hoped that this study will lead the development of nano-sized metal oxides with enhanced biocompatibility and sufficient structural properties with further research and modifications.

Author contribution All authors certify that they have participated sufficiently in the work to take public responsibility for the content. Moreover, each author certifies that this work has not been and will not be submitted to other journals or published in any other publication before. BY: investigation, methodology, data curation, writing original draft, and validation. LA: investigation, methodology, data curation, writing original draft, validation visualization, review, editing, and supervision. IEY: investigation, methodology, data curation, and validation. KS: investigation, methodology, data curation, writing original draft, and validation. MCA: investigation, methodology, data curation, and validation. DA: investigation, methodology, data curation, and validation. IIO: investigation, methodology, data curation, and validation. On behalf of all co-authors.

Funding This work was supported by the Scientific Research Project Coordination Center of Bahcesehir University (BAU) (Scientific Research Project Fund with the Project numbers BAP-2021.01.27 and BAP.2019–01.04).

Data availability All data generated or analyzed during this study are included in this published article.

Declarations

Competing interests The authors declare no competing interests.

References

1. Kaya S, Ozturk O, Arda L (2020) Roughness and bearing analysis of ZnO nanorods. Ceram Int 46(10):15183–15196
2. Senol SD, Yalcin B, Ozugurlu E, Arda L (2020) Structure, microstructure, optical and photocatalytic properties of Mn-doped ZnO nanoparticles. Materials Research Express 7(1):015079
3. Tosun M, Arda L (2019) Effect of temperature and film thickness on structural and mechanical properties of c-axis oriented $Zn_{0.95}Mg_{0.05}O$ thin films. Ceram Int 45(13):16234–16243
4. Suwanboon S, Amornpitoksuk P, Sukolrat A, Muensit N (2013) Optical and photocatalytic properties of La-doped ZnO nanoparticles prepared via precipitation and mechanical milling method. Ceram Int 39(3):2811–2819
5. Tania IS, Ali M (2021) Coating of ZnO nanoparticle on cotton fabric to create a functional textile with enhanced mechanical properties. Polymers 13(16):2701

6. Senol SD, Ozugurlu E, Arda L (2020) Synthesis, structure and optical properties of (Mn/Cu) co-doped ZnO nanoparticles. J Alloy Compd 822:153514
7. Arda L (2019) The effects of Tb doped ZnO nanorod: an EPR study. J Magn Magn Mater 475:493–501
8. Guler A, Arda L, Dogan N, Boyraz C, Ozugurlu E (2019) The annealing effect on microstructure and ESR properties of (Cu/Ni) co-doped ZnO nanoparticles. Ceram Int 45(2):1737–1745
9. Senol SD, Guler A, Boyraz C, Arda L (2019) Preparation structure and magnetic properties of Mn-doped ZnO nanoparticles prepared by hydrothermal method. J Supercond Novel Magn 32(9):2781–2786
10. Akcan D, Gungor A, Arda L (2018) Structural and optical properties of Na-doped ZnO films. J Mol Struct 1161:299–305
11. Boyraz C, Dogan N, Arda L (2017) Microstructure and magnetic behavior of (Mg/Ni) co-doped ZnO nanoparticles. Ceram Int 43(17):15986–15991
12. Gaikwad S, Garje V, Bansode A, Khot S, Choudhari V (2022) Evaluation of apoptotic and anti-cancer efficacy of microwave assisted (ZnO-Ag2O) hybrid nanoparticles in MCF-7 breast cancer cell lines. Inorg Chem Commun 139:109343
13. Parsa M, Entezari MH, Meshkini A (2021) Sonosynthesis approach improves anticancer activity of ZnO nanoparticles: reactive oxygen species depletion for killing human osteosarcoma cells. Nanomedicine 16(8):657–671
14. Donga S, Chanda S (2022) Caesalpinia crista seeds mediated green synthesis of zinc oxide nanoparticles for antibacterial, antioxidant, and anticancer activities. BioNanoScience 12(2):451–462
15. Sivakumar P, Lee M, Kim YS, Shim MS (2018) Photo-triggered antibacterial and anticancer activities of zinc oxide nanoparticles. J Mater Chem B 6(30):4852–4871
16. Yao C, Xiang F, Xu Z (2022) Metal oxide nanocage as drug delivery systems for Favipiravir, as an effective drug for the treatment of COVID-19: a computational study. J Mol Model 28(3):1–8
17. Anjum S, Hashim M, Malik SA, Khan M, Lorenzo JM, Abbasi BH, Hano C (2021) Recent advances in zinc oxide nanoparticles (ZnO NPs) for cancer diagnosis, target drug delivery, and treatment. Cancers 13(18):4570
18. Nigam A, Pawar SJ (2020) Synthesis and characterization of ZnO nanoparticles to optimize drug loading and release profile for drug delivery applications. Mater Today: Proc 20:2625–2628
19. Karakus S, Tan E, Ilgar M, Sahin YM, Mansuroglu DS, Ismik D, Kilislioglu A (2022) Swelling behaviour, rheological property and drug release profile of the anti-inflammatory drug metamizole sodium from xanthan gum–ZnO nanoparticles. Polym Bull 79(1):357–380
20. Ismail W, Bakry M, Elshobaki M, El-Shaer A, Abdelfatah M (2021) Impact of precursor concentrations and substrate type on properties of electrodeposited CdO nanorod thin films for optoelectronic applications. Mater Sci Semicond Process 133:105959
21. Zargar RA, Chackrabarti S, Malik MH, Hafiz AK (2021) Sol-gel syringe spray coating: a novel approach for Rietveld, optical and electrical analysis of CdO film for optoelectronic applications. Phys Open 7:100069
22. Alia AM, Mohammed AS, Hanfooshb SM (2021) The spectral responsivity enhancement for gallium-doped CdO/PS heterojunction for UV detector. J Ovonic Res 17(3):239–245
23. Srinivasan P, Prakalya D, Jeyaprakash BG (2020) UV-activated ZnO/CdO nn isotype heterostructure as breath sensor. J Alloy Compd 819:152985
24. Karthik K, Dhanuskodi S, Gobinath C, Prabukumar S, Sivaramakrishnan S (2017) Photocatalytic and antibacterial activities of hydrothermally prepared CdO nanoparticles. J Mater Sci: Mater Electron 28(15):11420–11429
25. Khan SA, Zahera M, Khan IA, Khan MS, Azam A, Arshad M, Elgorban AM (2022) Photocatalytic degradation of methyl orange by cadmium oxide nanoparticles synthesized by the sol-gel method. Optik 251:168401
26. Sperdouli I, Adamakis IDS, Dobrikova A, Apostolova E, Hanć A, Moustakas M (2022) Excess zinc supply reduces cadmium uptake and mitigates cadmium toxicity effects on chloroplast structure, oxidative stress, and photosystem II photochemical efficiency in Salvia sclarea Plants. Toxics 10(1):36
27. Heidari A (2022) Study of DNA/RNA aggregation linked to cadmium oxide (CdO) nanoparticles by aryl mercaptanes with various chain length. Earthline J Chem Sci 8(1):13–34
28. Heidari A, Brown C (2015) Study of composition and morphology of cadmium oxide (CdO) nanoparticles for eliminating cancer cells. J Nanomed Res 2:1–20
29. Mishra PK, Mishra H, Ekielski A, Talegaonkar S, Vaidya B (2017) Zinc oxide nanoparticles: a promising nanomaterial for biomedical applications. Drug Discov Today 22(12):1825–1834
30. Heidari A (2016) Novel and stable modifications of intelligent cadmium oxide (CdO) nanoparticles as anti–cancer drug in formation of nucleic acids complexes for human cancer cells' treatment. Biochem Pharmacol (Los Angel) 5(207):2167–501
31. Anandhan K, Harish S, Kumar RT (2019) Effect of morphology on the formation of CdO nanostructures for antibacterial and hemolytic studies. Appl Surf Sci 489:262–268
32. Prashanth GK, Prashanth PA, Bora U, Gadewar M, Nagabhushana BM, Ananda S, Sathyananda HM (2015) In vitro antibacterial and cytotoxicity studies of ZnO nanopowders prepared by combustion assisted facile green synthesis. Karbala Int J Mod Sci 1(2):67–77
33. Zhou X, Cao T (2022) Zinc oxide nanoparticle inhibits tumorigenesis of renal cell carcinoma by modulating lipid metabolism targeting miR-454-3p to repressing metabolism enzyme ACSL4. J Oncol
34. Berroukche A, Terras M, Labani A, Dellaoui H, Lansari W (2017) Effects of interaction CdZn on serum-PSA level and prostate histology in rats. Asian Pac J Trop Biomed 7(3):245–248
35. Bulat Z, Đukić-Ćosić D, Antonijević B, Buha A, Bulat P, Pavlović Z, Matović V (2017) Can zinc supplementation ameliorate cadmium-induced alterations in the bioelement content in rabbits? Arh Hig Rada Toksikol 68(1):38–44

36. Cai Y, Xu W, Wang M, Chen W, Li X, Li Y, Cai Y (2019) Mechanisms and uncertainties of Zn supply on regulating rice Cd uptake. Environ Pollut 253:959–965
37. Verdú I, Amariei G, Plaza-Bolaños P, Agüera A, Leganés F, Rosal R, Fernández-Piñas F (2022) Polystyrene nanoplastics and wastewater displayed antagonistic toxic effects due to the sorption of wastewater micropollutants. Sci Total Environ 819:153063
38. Chandler JD, Wongtrakool C, Banton SA, Li S, Orr ML, Barr DB, Jones DP (2016) Low-dose oral cadmium increases airway reactivity and lung neuronal gene expression in mice. Physiol Rep 4(13):e12821
39. Brys M, Nawrocka AD, MlekoŚ E, Zydek C, Foksinski M, Barecki A, Krajewska WM (1997) Zinc and cadmium analysis in human prostate neoplasms. Biol Trace Elem Res 59(1–3):145–152
40. Jacquillet G, Barbier O, Cougnon M, Tauc M, Namorado MC, Martin D, Poujeol P (2006) Zinc protects renal function during cadmium intoxication in the rat. Am J Physiol-Renal Physiol 290(1):F127–F137
41. Barbier O, Dauby A, Jacquillet G, Tauc M, Poujeol P, Cougnon M (2005) Zinc and cadmium interactions in a renal cell line derived from rabbit proximal tubule. Nephron Physiol 99(3):74–84
42. Zhang H, Zhang W, Huang S, Xu P, Cao Z, Chen M, Lin X (2022) The potential role of plasma membrane proteins in response to Zn stress in rice roots based on iTRAQ and PRM under low Cd condition. J Hazard Mater 429:128324
43. Zhu Y, Qiu W, Li Y, Tan J, Han X, Wu L, Zhuo R (2022) Quantitative proteome analysis reveals changes of membrane transport proteins in Sedum plumbizincicola under cadmium stress. Chemosphere 287:132302
44. Toušová Z, Kuta J, Hynek D, Adam V, Kizek R, Bláha L, Hilscherová K (2016) Metallothionein modulation in relation to cadmium bioaccumulation and age-dependent sensitivity of Chironomus riparius larvae. Environ Sci Pollut Res 23(11):10504–10513
45. Rogalska J, Pilat-Marcinkiewicz B, Brzóska MM (2011) Protective effect of zinc against cadmium hepatotoxicity depends on this bioelement intake and level of cadmium exposure: a study in a rat model. Chem Biol Interact 193(3):191–203
46. Bulat ZP, Djukić-Ćosić D, Maličević Z, Bulat P, Matović V (2008) Zinc or magnesium supplementation modulates Cd intoxication in blood, kidney, spleen, and bone of rabbits. Biol Trace Elem Res 124(2):110–117
47. Poli V, Madduru R, Aparna Y, Kandukuri V, Motireddy SR (2022) Amelioration of cadmium-induced oxidative damage in Wistar rats by vitamin C, zinc and N-acetylcysteine. Med Sci 10(1):7
48. Domouky AM, Abdel-Kareem RH, El-wafaey DI (2022) Zinc supplementation attenuates cadmium induced jejunal injury in adult male albino rats: histopathological and biochemical study. Zagazig Univ Med J 28(2):364–378
49. Refat MS, Hamza RZA, Adam AM, Saad HA, Gobouri AA, Azab E, El-Megharbel SM (2021) Antioxidant, antigenotoxic, and hepatic ameliorative effects of quercetin/zinc complex on cadmium-induced hepatotoxicity and alterations in hepatic tissue structure. Coatings 11(5):501
50. Kwiecień M, Winiarska-Mieczan A, Milczarek A, Tomaszewska E, Matras J (2016) Effects of zinc glycine chelate on growth performance, carcass characteristics, bone quality, and mineral content in bone of broiler chicken. Livest Sci 191:43–50
51. Yang WL, Chen YP, Cheng YF, Li XH, Zhang RQ, Wen C, Zhou YM (2016) An evaluation of zinc bearing palygorskite inclusion on the growth performance, mineral content, meat quality, and antioxidant status of broilers. Poult Sci 95(4):878–885
52. Ong GH, Yap CK, Maziah M, Tan SG (2013) Synergistic and antagonistic effects of zinc bioaccumulation with lead and antioxidant activities in centella asiatica. Sains Malays 42(11):1549–1555
53. Zhen S, Shuai H, Xu C, Lv G, Zhu X, Zhang Q, …, Huang D (2021) Foliar application of Zn reduces Cd accumulation in grains of late rice by regulating the antioxidant system, enhancing Cd chelation onto cell wall of leaves, and inhibiting Cd translocation in rice. Sci Total Environ 770:145302
54. Li X, Lu H, Zhang Y, He F (2017) Efficient removal of organic pollutants from aqueous media using newly synthesized polypyrrole/CNTs-CoFe2O4 magnetic nanocomposites. Chem Eng J 316:893–902
55. Yalçın B, Erbil C (2018) Effect of sodium hydroxide solution as polymerization solvent and activator on structural, mechanical and antibacterial properties of PNIPAAm and P (NIPAAm–clay) hydrogels. Polym Compos 39:E386–E406
56. Spencer JA, Mock AL, Jacobs AG, Schubert M, Zhang Y, Tadjer MJ (2022) A review of band structure and material properties of transparent conducting and semiconducting oxides: Ga_2O_3, Al_2O_3, In_2O_3, ZnO, SnO_2, CdO, NiO, CuO, and Sc_2O_3. Appl Phys Rev 9(1):011315
57. Rana N, Chand S, Gathanian AK (2015) Tailoring the structural and optical properties of ZnO by doping with Cd. Ceram Int 41(9):12032–12037
58. Chan YB, Selvanathan V, Tey LH, Akhtaruzzaman M, Anur FH, Djearamane S, Aminuzzaman M (2022) Effect of calcination temperature on structural, morphological and optical properties of copper oxide nanostructures derived from Garcinia mangostana L. leaf extract. Nanomaterials 12(20):3589
59. Patra T, Mohanty A, Singh L, Muduli S, Parhi PK, Sahoo TR (2022) Effect of calcination temperature on morphology and phase transformation of MnO_2 nanoparticles: a step towards green synthesis for reactive dye adsorption. Chemosphere 288:132472
60. Bari ML, Sonawane SH, Mishra S, Deshpande TD (2023) Surfactant assisted reactive crystallization of cobalt oxide nanoparticles in a tubular microreactor: effects of precursor concentrations and type of surfactants. React Chem Eng 8:355–364
61. Esakki ES, Vivek P, Sundar SM (2023) Influence on the efficiency of dye-sensitized solar cell using Cd doped ZnO via solvothermal method. Inorg Chem Commun 147:110213
62. Al-Hada NM, Mohamed Kamari H, Abdullah CAC, Saion E, Shaari AH, Talib ZA, Matori KA (2017) Down-top nanofabrication of binary $(CdO)_x(ZnO)_{1-x}$ nanoparticles and their antibacterial activity. Int J Nanomed 12:8309–8323
63. Reddy CV, Babu B, Shim J (2018) Synthesis, optical properties and efficient photocatalytic activity of CdO/ZnO hybrid nanocomposite. J Phys Chem Solids 112:20–28

64. Najim JA, Rozaiq JM (2013) Effect Cd doping on the structural and optical properties of ZnO thin films. Int Lett Chem Phys Astron 10:137–150
65. Rana N, Chand S, Gathania AK (2015) Tailoring the structural and optical properties of ZnO by doping with Cd. Ceram Int 41(9):12032–12037
66. Zargar RA, Shah AH, Arora M, Mir FA (2019) Crystallographic, spectroscopic and electrical study of ZnO: CdO nanocomposite-coated films for photovoltaic applications. Arab J Sci Eng 44(7):6631–6636
67. Markiewicz KH, Zembko P, Półtorak K, Misztalewska I, Wojtulewski S, Majcher AM, Wilczewska AZ (2016) Magnetic nanoparticles with chelating shells prepared by RAFT/MADIX polymerization. New J Chem 40(11):9223–9231
68. Li HC, Hsieh FJ, Chen CP, Chang MY, Hsieh PC, Chen CC, Chang HC (2013) The hemocompatibility of oxidized diamond nanocrystals for biomedical applications. Sci Rep 3:3044
69. Zhang H (2016) Erythrocytes in nanomedicine: an optimal blend of natural and synthetic materials. Biomater Sci 4(7):1024–1031
70. Drag-Kozak E, Kuchta-Gładysz M, Grzesiakowska A, Łuszczek-Trojnar E, Socha M (2022) Genotoxic effect of cadmium and zinc in the peripheral erythrocytes of *Prussian carp (B.)*. J Vet Res 66:619–628
71. Kumari D, Garg S, Bhawrani P (2022) Zinc homeostasis in immunity and its association with preterm births. Scand J Immunol 95(4):e13142
72. Adelakun SA, Ogunlade B, Fidelis OP, Omotoso OD (2022) Protective effect of nutritional supplementation of zinc-sulfate against cisplatin-induced spermatogonial and testicular dysfunctions in adult male Sprague-Dawley rats. Endocr Metab Sci 6:100116
73. Sloup V, Jankovská I, Štolcová M, Magdálek J, Karešová V, Lanková S, Langrová I (2021) Effects of excessive dietary zinc or zinc/cadmium and tapeworm infection on the biochemical parameters in rats. J Anim Physiol Anim Nutr 105(5):989–995
74. Jaeschke H, Ho YS, Fisher MA, Lawson JA, Farhood A (1999) Glutathione peroxidase–deficient mice are more susceptible to neutrophil-mediated hepatic parenchymal cell injury during endotoxemia: importance of an intracellular oxidant stress. Hepatology 29(2):443–450
75. El-Kenawi A, Ruffell B (2017) Inflammation, ROS, and mutagenesis. Cancer Cell 32(6):727–729
76. Nagarajan M, Maadurshni GB, Tharani GK, Udhayakumar I, Kumar G, Mani KP, Manivannan J (2022) Exposure to zinc oxide nanoparticles (ZnO-NPs) induces cardiovascular toxicity and exacerbates pathogenesis–role of oxidative stress and MAPK signaling. Chem Biol Interact 351:109719
77. Fakhri A, Behrouz S (2015) Photocatalytic properties of tungsten trioxide (WO_3) nanoparticles for degradation of Lidocaine under visible and sunlight irradiation. Sol Energy 112:163–168
78. Vinardell MP, Sordé A, Díaz J, Baccarin T, Mitjans M (2015) Comparative effects of macro-sized aluminum oxide and aluminum oxide nanoparticles on erythrocyte hemolysis: influence of cell source, temperature, and size. J Nanopart Res 17(2):1–10
79. Yadav S, Maurya PK (2022) Recent advances in the protective role of metallic nanoparticles in red blood cells. Biotech 12(1):1–13
80. Madan R, Kumar V, Mohan D (2022) Structural and morphological properties of pristine and Zn doped CdO nanoparticles for thermoelectric applications. Mater Today: Proc 54:664–668
81. Zhang D, Zeng F (2012) Visible light-activated cadmium-doped ZnO nanostructured photocatalyst for the treatment of methylene blue dye. J Mater Sci 47:2155–2161
82. Ghoderao KP, Jamble SN, Kale RB (2019) Hydrothermally synthesized Cd-doped ZnO nanostructures with efficient sunlight-driven photocatalytic and antibacterial activity. J Mater Sci: Mater Electron 30:11208–11219
83. Masood A, Iqbal T, Ashraf M, Nazir A, Ali F, Ranjha QA, Galal AM (2023) Synthesis and characterization of cadmium doped zinc oxide nanoparticles for visible light driven catalytic removal of MB and RhB dye: experimental and computational analysis. J Inorgan Organomet Polym Mater 2023:1–14
84. Phuruangrat A, Mad-Ahin S, Yayapao O, Thongtem S, Thongtem T (2015) Photocatalytic degradation of organic dyes by UV light, catalyzed by nanostructured Cd-doped ZnO synthesized by a sonochemical method. Res Chem Intermed 41:9757–9772
85. Dumrongrojthanath P, Phuruangrat A, Thongtem S, Thongtem T (2021) Photocatalysis of Cd-doped ZnO synthesized with precipitation method. Rare Met 40:537–546
86. Zhai YJ, Li JH, Fang X, Chen XY, Fang F, Chu XY, …, Wang XH (2014) Preparation of cadmium-doped zinc oxide nanoflowers with enhanced photocatalytic activity. Mater Sci Semicond Process 26:225–230